Self-organized nickel nanoparticles on nanostructured silicon substrate intermediated by a titanium oxynitride (TiN_xO_y) interface

M. Morales, R. Droppa, S. R. S. de Mello, C. A. Figueroa, A. R. Zanatta, and F. Alvarez

Citation: AIP Advances **8**, 015025 (2018);
View online: https://doi.org/10.1063/1.4993143
View Table of Contents: http://aip.scitation.org/toc/adv/8/1
Published by the American Institute of Physics

Self-organized nickel nanoparticles on nanostructured silicon substrate intermediated by a titanium oxynitride (TiN_xO_y) interface

M. Morales,[1] R. Droppa, Jr.,[2] S. R. S. de Mello,[3] C. A. Figueroa,[3] A. R. Zanatta,[4] and F. Alvarez[1,a]

[1]*Instituto de Física 'Gleb Wataghin', Universidade de Campinas (UNICAMP), 13081-970 Campinas, SP, Brazil*
[2]*Centro de Ciências Naturais e Humanas, Universidade Federal do ABC, 09.210-580 Santo André, SP, Brazil*
[3]*Programa de Pós-Graduação em Engenharia e Ciências dos Materiais (PGMAT), Universidade de Caxias do Sul (UCS), 95070-560 Caxias do Sul, RS, Brazil*
[4]*Instituto de Física de São Carlos (IFSC), Universidade de São Paulo (USP), 13566-590 São Carlos, SP, Brazil*

(Received 27 June 2017; accepted 15 January 2018; published online 25 January 2018)

In this work we report an experimental approach by combining in situ sequential top-down and bottom-up processes to induce the organization of nanosized nickel particles. The top-down process consists in xenon ion bombardment of a crystalline silicon substrate to generate a pattern, followed by depositing a ~15 nm titanium oxynitride thin film to act as a metallic diffusion barrier. Then, metallic nanoparticles are deposited by argon ion sputtering a pure nickel target, and the sample is annealed to promote the organization of the nickel nanoparticles (a bottom-up process). According to the experimental results, the surface pattern and the substrate biaxial surface strain are the driving forces behind the alignment and organization of the nickel nanoparticles. Moreover, the ratio between the F of metallic atoms arriving at the substrate relative to its surface diffusion mobility determines the nucleation regime of the nickel nanoparticles. These features are presented and discussed considering the existing technical literature on the subject. https://doi.org/10.1063/1.4993143

I. INTRODUCTION

Nickel nanoparticles are commonly used as catalysts for growing carbon nanotubes CNT that, because of their unique characteristics, require very specific production-processing conditions[1–7] Most of the work involving the Ni-CNT system relies on expensive (top-down process) substrate preparation such as X-ray and laser interference lithography.[1] Looking for simpler and less expensive methods, self-organized templates have been reported as viable routes to substitute these top-down processes.[8] Within them, the formation of (nanostructured) patterns by bombarding glasses, metals, as well as semiconductor substrates with noble gases are very promising.[9] By using this technique, Oates *et al.* reported the achievement of aligned carbon nanowires, after ion bombarding crystalline silicon substrates.[10] The phenomena taking place in the formation of such (patterned) substrates is an attractive subject and involves the diffusion and coalescence of the catalyst particles. An excellent review on the subject was recently published by Muñoz-Garcia and coworkers.[11]

In these processes, the substrate can influence the development of strain altering the composition of the nanoparticles. For instance, templates based on silicon substrates is the unintentional formation of silicide compounds. Towards this end, titanium dioxide[8] and silicon dioxide[10] are

[a]Corresponding Author Tel.: +55-19992042313; fax: 55 19 35215372; e-mail: alvarez@ifi.unicamp.br

efficient barriers that prevent the diffusion of metal particles into the silicon substrate. An alternative approach adopted in the present contribution, involves the use of titanium oxynitride (TiN_xO_y) thin films which, additionally, presents low residual stress, good thermal-electrical conductivity, and is compatible with the fabrication of devices.[12] Regarding the strain, it is well-known that ions arriving at the substrate with enough energy (>100 eV) are implanted giving rise to stress.[13–17] A typical example involves xenon atoms that, because of their large sizes, occupy smaller places inside the silicon lattice inducing stress in the network outwards and parallel to the silicon surface by the knock-on process. Whilst the atomic lattice is free to expand perpendicularly to the sample surface, an expansion parallel to its plane is not allowed, so inducing a macroscopic in-plane biaxial stress.[16]

Motivated by these aspects, in this work we propose and discuss a sequential top-down and bottom-up processing combined with ion beam deposition to produce a regular pattern of nickel nanoparticles.[1,18,19] The top-down process consists in xenon ion bombarding a crystalline silicon substrate to generate a regular pattern, over which is deposited a ~15 nm thick TiN_xO_y thin film that will act as a diffusion barrier. Sequentially, metallic nanoparticles are deposited by argon ion sputtering a pure nickel target, and the sample is annealed to promote the organization of the nickel nanoparticles (bottom-up process). Then, the influence of some experimental conditions onto the arrangement of the nickel nanoparticles was investigated by different experimental techniques. According to the literature, the surface diffusion coefficient D (cm^2s^{-1}) and the flux of nickel atoms F (particles cm^{-2} s^{-1}) arriving to the substrate are the most important parameters controlling the nickel nanoparticles surface density. More specifically, the density of islands nucleation is given by r ($1/cm^2$) $\sim F^p/D^q$.[1–21] The diffusion coefficient D depends on temperature while p and q are positive parameters depending on the nucleation mechanisms. The diffusion coefficient is given by the Einstein classic equation $D = L^2/\tau$, where L and τ stand for the mean distance traveled by the atoms and the lifetime of an adsorbed atom before being re-evaporated, respectively.[22] We shall see that the lifetime τ have an important role explaining the effect of the nickel coalescence on the silicon substrate. Roughly speaking, atoms landing on the substrate wander around the surface before nucleation or re-evaporation. For constant F and large values of D the number of islands nucleation r ($1/cm^2$) is low. For constant F and smaller D, the density of islands nucleation r ($1/cm^2$) increases.[1,20,21] In the former case, the nucleation occurs under near thermodynamic equilibrium, *i.e.*, added atoms have enough time to reach an equilibrium position. In the latter, the process takes place under non-equilibrium conditions and the atoms nucleate in metastable sites.[1] Regarding the self-organized arrangement of nanoparticles at scales larger than the atomic distances, the driving forces of long range are intervening as, for instance, electric, magnetic or elastic ones.[1] Therefore, in this work, the strain induced by the ion bombardment will be considered such that the organization of the nanoparticles can be analyzed taking into account the driving forces of both short and long distances, the ratio $r \sim F^p/D^q$, and the strain present in the substrate.

To gain further insight on the mechanisms behind the development of the self-organized nickel nanoparticles, a mirror polished (non-structured) crystalline silicon substrate was prepared and investigated in detail as well.

II. EXPERIMENTAL

A. Sample preparation

The samples were prepared in a high vacuum system containing two Kaufman ion cells (Dual Ion Beam Assisted Deposition, DIBAD) attached to a UHV chamber for in situ XPS measurements. One of the cells is used to sputter a solid target (either Ti or Ni metal in the present work) and the other to bombard the substrate-sample. The sample is ~20 cm distant from the targets holder, which consists in a cube that can be manually rotated to select the desired target.[23] During deposition, the surface of the sample was kept parallel to the surface of the target: Ti (99.9995 % pure) for the TiN_xO_y film and Ni (99.9995 %) for the nickel nanoparticles. Whereas the experimental apparatus allows to select the incidence angle, energy and current of the Xe^+ ions during the patterning process, we have not direct information concerning the Ni atoms reaching the Si substrate.

P-type (B-doped 1-10 Ω cm), mirror polished, (100)-oriented crystalline silicon substrates were considered in the whole procedure.

Based on AFM measurements, the surface of the pristine (non-structured) Si substrates is rather smooth, with average roughness values orders of magnitude smaller than that exhibited by the structured samples. Prior processing-deposition, the Si substrates were cleaned by blowing N_2 (99.995 %) and their native oxide upper layer removed after a few seconds Ar^+ ion bombarding procedure, as clearly indicated by XPS measurements.

The preparation of the structured samples comprised the bombardment of a Si substrate with Xe^+ ions (500 eV and 99.999 %), as provided by one of the Kaufman cells. The process was 30 min long and the Xe^+ ions hit the Si substrate at 15^0 incident angles [Figures 1(a) and 1(b)]. In these experimental conditions the chamber pressure is ~$1x10^{-2}$ Pa and the absolute Xe^+ ion density at the Si substrate (as obtained from a Faraday cup located in the substrate) was ~1 mA/cm^2. As expected, ion bombardment prompted a characteristic pattern thought that some flaws are evident, as shown in Figure 1(c) and in previous work.[24] Ion bombardment also originated an amorphous top-layer followed by a ripple stressed crystalline interface.[11,25–27] The characteristics of such amorphous top-layer can be inferred by using the SRIM program[28] along with the Xe^+ ion energy (500 eV) and angle of incidence (15^0). The simulation shows that the ion ranges and straggle are ~2.9 nm and ~0.6 nm, respectively, indicating an amorphous Si top-layer of the order of (2.9 ± 0.6) nm.

Afterwards, a TiN_xO_y thin film [yellow, Figure 1(d)] was deposited using the second Kaufman cell by sputtering the Ti target with an Ar^+ ion beam (1450 eV and ~5 mA/cm^2). The reactive atmosphere was constituted by N_2 (~10^{-2} Pa) and O_2 (~10^{-5} Pa) and the deposition was 5 min long, rendering a ~15 nm thick film. Following a ~1 keV Ar^+ beam, the energy of the ejected Ti species stays in the 1-15 eV range, suggesting that the resputtering of the TiN_xO_y film is negligible.[29] The AFM image of the sample after substrate structuring and TiN_xO_y deposition is shown in Figure 1(e), in which the golden color is an artifact to enlighten the ripples. The (in situ) XPS measurements of the TiN_xO_y films deposited on both structured and non-structured samples indicate very similar results, *i.e.*, [O] = (7.3±0.5), [Ti] = (45.1±0.5) and [N] = (47.5±0.5) at.%. Also, the TiN_xO_y are polycrystalline and texturized (Figure 2). Sample preparation continues by Ar^+ ion bombarding the Ni target (nominal ion density ~5 mA/cm^2), such that the number of Ni atoms reaching the Si substrate is determined by the Ar^+ ion characteristics. Finally, the samples were thermally annealed to promote the nucleation and/or coalescence of Ni nanoparticles. The uniformity of the metallic particles (Ti or Ni) arriving to the substrate was estimated, indirectly, by measuring the thickness of the TiN_xO_y or Ni films (~15nm) by AFM. The thickness proved to be constant within ~2-3 % suggesting that the F of incident particles is quite uniform relative to the sample size (1x2 cm^2). Finally, we note that two sets of samples were specifically prepared for the study under specific conditions of ion beam energy bombarding and substrate temperature, as explained in detail below.

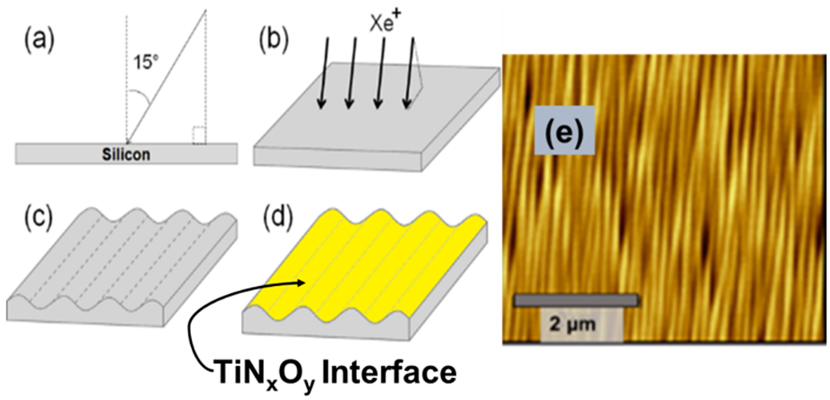

FIG. 1. Scheme of the sequential steps of Xe^+ ion bombardment (from a to c – top-down process) and after deposition of the titanium-based interface (yellow) (d). AFM image of a typical Si wafer nanostructured by the ion bombardment (e) (the golden color is an artifact to enlighten the ripples.

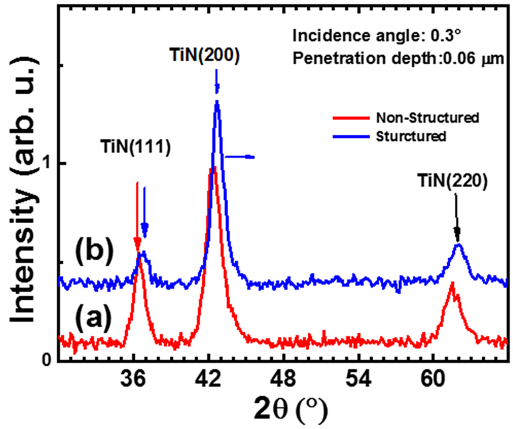

FIG. 2. GIXRD measurements obtained from TiN_xO_y coated (a) non-structured and (b) structured Si substrates (adapted from Ref. 24).

1. Influence of the temperature on the nickel diffusion coefficient (Set A)

In this set of samples, Ni particles were deposited at 500, 600, and 700 ^{0}C on both structured and non-structured substrates intermediated by a TiN_xO_y film (Table I). The films were obtained by bombarding the Ni target with 1 keV Ar^+ ions during 1 min and annealed by 2 min at the very same deposition temperature. Considering a background pressure of 10^{-5} Pa, we should consider that oxidation of the Ni particles is probably taking place during the process of coalescence. However, within the experimental error, the XPS spectrum of the Ni 2p core level (not shown) does not show evidence of the Ni^{2+} chemical state, which is characteristic of NiO species. Nevertheless, the oxidation of the outermost layer of the Ni particles cannot be rule out.

2. Influence of the nickel F (Set B)

Nickel particles were deposited on structured and non-structured Si substrates covered with TiN_xO_y, at 700 and 500°C, for 1 min, with energies spanning from 200 to 1000 eV (Table II). The annealing procedure was the same as before.

We note that, to be able to compare island densities, the same amount of material should be deposited and retained on the substrate. As explained below, the amount of material deposited can be obtained by adjusting the Ni dose, i.e., controlling the deposition time of the metal. However, it is difficult to perform for different substrate temperatures because re-evaporation effects. Only at relative low temperatures of deposition, where re-evaporation is negligible, allows to consider constant the amount of metal on the surface. Therefore, the results report information from a combined effect of the surface diffusion and evaporation of Ni atoms.

TABLE I. Parameters used for the Ni particles deposition on TiN_xO_y/Si structured and non-structured substrates (Set A). The samples were obtained by Ar^+ ion beam bombarding a pure Ni target (99.9995 %, 1 keV beam energy) during 1 min at the temperatures indicated. Afterward, annealing treatments were pursued during 2 min at the same temperatures used in the deposition.

Set A	Sample	Temperature (°C)
non-structured	A1	500
	A2	600
	A3	700
structured	A4	500
	A5	600
	A6	700

TABLE II. Nickel deposition parameters on the nanostructured TiN_xO_y coated non-structured and structured silicon substrates (Set B). The F of Ni atoms increases with the sputtering energy.

Set B	Sample	Temperature (°C)	Energy (eV)
non-structured	BC1	500	1000
	BC2	”	800
	BC3	”	600
	BC4	”	400
	CC5	”	200
structured	B1	700	1000
	B2	”	800
	B3	”	600
	B4	”	400
	B5	”	350
	B6	”	200

B. Sample characterization

The strains of the TiN_xO_y polycrystalline films deposited on the Si substrates were obtained by measuring the 2θ position of the TiN (200) Bragg reflection in in-plane grazing incidence X-ray diffraction (GIXD) geometry for 8 azimuthal angles ϕ in steps of 45°. The residual strains of the films were evaluated by:

$$\varepsilon = \frac{d - d_0}{d_0} = \frac{\sin(\frac{2\theta_0}{2})}{\sin(\frac{2\theta}{2})} - 1, \quad (1)$$

where $2\theta_0$ is the angle associated with the (200) Bragg reflection of the relaxed TiN_xO_y film. The convenient expression of the strain ε in the above equation is obtained by substituting d (d_0) by the Bragg condition $n\lambda = 2d \sin\theta$ ($n\lambda = 2d_0 \sin\theta_0$). To complete the characterization, polar stress maps of the studied samples were obtained. To do this, series of X-ray diffraction measurements in the θ-2θ configuration were performed using the same experimental setup. The measurement was performed focusing on the (200) main reflection associated with the TiN_xO_y intermediate thin film by monitoring different positions of the substrate and rotating the sample around its azimuthal angle.

The diffraction measurements were performed on the XRD2 beamline at the Brazilian Synchrotron Light Source (LNLS, Campinas, SP, Brazil). This beamline is constituted by a double bounce sagittal focusing (111)-Si monochromator and a 4+2-circle Huber diffractometer. The energy of the X-ray beam was 8.04 keV (λ= 0.1520 nm) close to the Cu $K_{\alpha 1}$ line. The detector aperture was 1.0 $mm^{Vertical}$ x 20 $mm^{Horizontal}$ located at 1100 mm from the sample, resulting in a resolution of 0.9 mrad in 2θ.

For the study of the Ni particles surface diffusion, basically two techniques were employed: a) surface topographic characterizations by Atomic Force Microscopy (AFM, Innova-Vecco) performed in tapping mode; and b) a surface chemical composition by X-ray photoelectron spectroscopy (XPS) in the ultra-high vacuum system attached to the preparation chamber, *i.e.*, the studies are performed without exposing the samples to the atmosphere (see Section II) The XPS measurements were carried out by means of 1486.6 eV photons from an Al target (Kα line, Thermo Alpha 110 Hemispherical Analyzer). The apparatus total resolution was ~0.85 eV (natural Kα line-width plus analyzer characteristics). It is important to remark that with the energy of the used photons, the XPS technique probes up to ~ 5-30 Å sample depths.[30] As the goal of the study is associated with surface phenomena, the physical information extracted by the technique is adequate. Finally, to obtain the size and distribution of the nickel particles on the substrates, their surfaces were examined and analyzed by Scanning Electron Microscopy (FEG-SEM, Quanta 650FEG).

III. RESULTS AND DISCUSSION

A. Introduction

Several theories and models have been proposed to explain the phenomenon of formation of regular patterns in metals and semiconductors bombarded by heavy ions. As commented in Section I, Muñoz-Garcia *et al.* published a complete review on the formation of ripples in solids by ion beam bombardment.[11] Details of these phenomena are exhaustively discussed in the cited work and here we shall briefly comment some causes prompting the formation of regular patterns. Effects of preferential sputtering, surface diffusion of added atoms, the presence of impurities, and defects are commonly invoked to explain the reported results in the formation of regular patterns originated by ion bombardment.[11,31–35] Roughly speaking, the regular pattern stems from mechanisms inducing surface instability such as surface local curvature dependence of the ion sputtering yield, presence of energy barriers hindering added atoms to diffuse overstep edges, surface mass redistribution, as well as materials structure.[11] Indeed, in a crystalline semiconductor like Si, the stiff covalent directional bonds hinder atoms motion and the ripples generally follow the direction of the ion beam. The non-directional bonds character in metals, on the other hand, allows added atoms to accommodate and the ripples tend to follow the material crystalline orientation.[9] Under the substrate preparation conditions presented in Section II, the wavelength of the obtained ripples was ~180 nm following a direction quite parallel to the ion beam projection on the sample substrate. This periodicity was the "standard" optimized substrate preparation in our labs.

B. Grazing incidence x-ray diffraction characterization of the TiN_xO_y thin film deposited on structured and non-structured Si substrates

From the AFM topographic measurements (not shown) we confirmed that the TiN_xO_y film (15 nm thick) preserves the topography of the substrate, *i.e.*, the coating accompanies the shapes, being flat or corrugated, in the case of non-structured or structured Si substrates, respectively. Previously, we have reported that the ripples wavelength of both naked and TiN_xO_y coated structured Si are equivalent within the experimental errors.[24] In the cited reference, we have discussed the strain in non-structured (i.e., pristine) and structured Si substrates. Now, we proceed to study the strain of the TiN_xO_y-Si interface deposited on differently treated silicon substrates. As remarked in Section I, the stress and topography of the TiN_xO_y thin film used to host the Ni particles are important to understand the self-organization of the metallic Ni reported in this paper.

Figure 2 shows the diffractograms obtained from TiN_xO_y films deposited on Si (non-structured) substrates, as previously reported.[24] The following conclusions can be drawn from this plot. First, the reflections associated with TiN of the structured substrate shift to higher angle values indicating a stressed TiN_xO_y film. Second, the different $I_{(200)}/I_{(111)}$ intensity ratios (*i.e.*, the texture) in the diffractograms (a) and (b) is caused by the nanostructured substrate on TiN_xO_y films. Finally, the TiN_xO_y films adopted the preferential (200) orientation as was already reported by Narayan et al.[36]

C. Polar strain graphs of the TiN_xO_y films on (non-)structured Si substrates

As remarked in Section II, among other effects, ion bombardment prompts strain. To characterize this effect, the in-plane polar strain graphs of the studied TiN_xO_y films were obtained. Figure 3 represents the strain on plane polar graphs stemming from X-rays studies of TiN_xO_y calculated by the equation $\varepsilon = \frac{d-d_0}{d_0}$ (Section II). The plots correspond to the (200) Si diffraction peak and show the lattice distortion stress introduced on the TiN_xO_y films deposited on the structured Si substrate as compared with the film deposited on the non-structured one. We note that the "bird peak" in the polar graphs are artifacts stemming from the data processing at the point where the curves joint. Figure 4 displays the Normalized Polar Strain (NPS) plot corresponding to the curves displayed in Figure 3. We note that an anisotropic strain is present in both types of samples, even in the coated non-structured substrate. The anisotropic strain stems from the effect of the ripples on the oxynitride films and the stress generated by the ion bombarding process.[16,17] This is also probably associated with the patterns flaws and the fact that the ripples are not forming perfect parallel grooves.

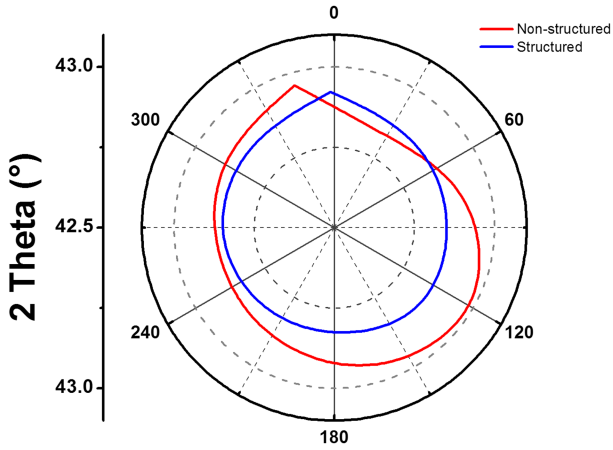

FIG. 3. Polar graph showing the position of the (200) reflection from the studied films. The "bird beaks" observed in the polar graphs are artifacts stemming from the data processing at the point where the curves joint.

The NPS plot for the non-structured Si is preferentially oriented along the 120°-300° direction. On the other hand, the NPS plots of the samples deposited on the structured substrate show characteristic elongations in the 0° to 120° direction (Figure 3). Therefore, we can conclude that the TiN_xO_y films deposited on the structured substrates prompt a lattice "redistribution" of the original stress (Figure 4). Finally, we note that this figure suggests that the polar shape is a combination of both the original and the strain prompted by the patterning process influenced by the characteristics of the TiN_xO_y-Si interface.[36]

D. Ni particles organization

As discussed in Section I, the self-organization of the Ni particles depends on the diffusion (D) of added atoms and the F of atoms arriving at the substrate, *i.e.*, on the F^p/D^q ratio. Also, for distances larger than the atomic ones, the importance of elastic forces (strain) are important.[1] Therefore, in

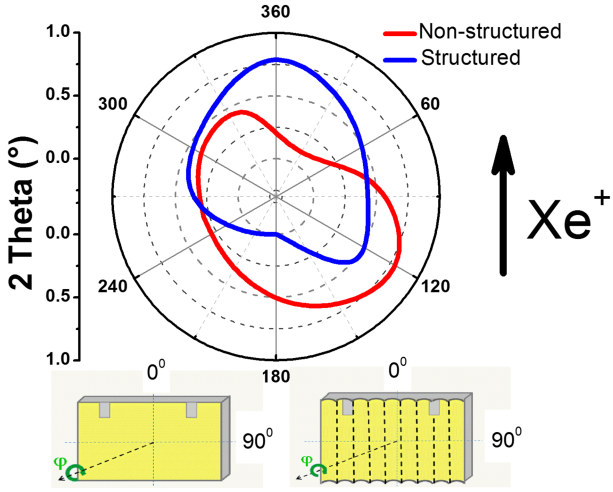

FIG. 4. Top Panel: Normalized Polar Strain (NPS) plots corresponding to TiN_xO_y interface deposited on non-structured and structured Si substrates. The former NPS is preferentially oriented in the 120°-300° direction while the later one shows elongations along the 0°-120° orientation. Bottom Panel: schematic representation of the samples indicating the rotation angle φ around the z-axis perpendicular to the surface. The two top gray marks correspond to the clamps used to fix the Si samples on the substrate holder and were used as position guides during the deposition experiments. The projection of the Xe^+ ion beam on the surface sample is the vertical axis passing by 0° in both plots.

this section we shall discuss two main subjects. First, the diffusion and coalescence properties of nickel on the two types of Si substrates, namely, structured and non-structured (sub-sections 1, 2 and 3). Second, the organization and distribution of the Ni particles dependence on both types of studied substrates as a function of temperature T and particle F (sub–section 4). The former study is important to identify the dominant mechanism on the displacement and coalescence of Ni atoms. Indeed, these experiments revealed that the strain and topology of the substrates play an important role on the nucleation and/or coalescence sites of the Ni particles. In other words, both the elastic forces stemming from the substrate strain and atoms diffusion influence the mesoscale and atomic scales of dislocation of Ni atoms intervening in the organization of Ni particles.

1. Influence of T and the substrate topography on Ni atoms diffusion

In a previous paper, we reported self-organized nickel nanoparticles deposited on nanostructured Si wafers intermediated with TiN_xO_y films at both constant temperature T and Ni atoms F.[24] In this section, we pursued a further investigation of the phenomenon by systematically studying the diffusion of Ni atoms deposited on nanostructured substrates as a function of temperature T (sample Set A, Section II A, Table I) and atoms F (sample Set B, Section II A, Table II).

With the purpose of studying the effect of T on the surface diffusion of Ni atoms, the F of Ni was maintained constant by fixing the energy of the sputtering ion Ar^+ beam at 1 keV. Then, the Ni target was sputtered during 1 min for all the studied samples at different substrate temperatures (Table I). Afterward, in-situ annealing treatment at the same T used during the Ni deposition was performed at $\sim 10^{-5}$ Pa. The deposition temperatures used in the experiments have been chosen based on previous works reporting changes in the diffusion kinetics of Ni atoms between 400-1000 ^{0}C.[37,38]

Figure 5 shows the Ni concentration plotted as ln[Ni] versus 10^3/T for the studied samples. The open triangles and squares indicate the surface concentration of Ni in arbitrary units obtained from the XPS measurements. First, we note that the relative amount of Ni remaining on the substrate at different deposition temperatures results from a competition of Ni atoms diffusion until they reach a nucleation center, meet other particles to form islands, or detach and re-evaporate.

Second, the fact that in both cases the concentration of Ni decreases with increasing T (Fig. 5), suggests that the evaporation rate is a mechanism competing with the particles nucleation and growth process, *i.e.*, one can assume that the nickel concentration [Ni] is proportional to the metallic atoms mean lifetime evaporation $\tau = \tau_0 \exp(W/k_BT)$, where W is the activation evaporation energy per atom, k_B the Boltzmann constant, and T (absolute temperature). The pre-factor τ_0 is related to the

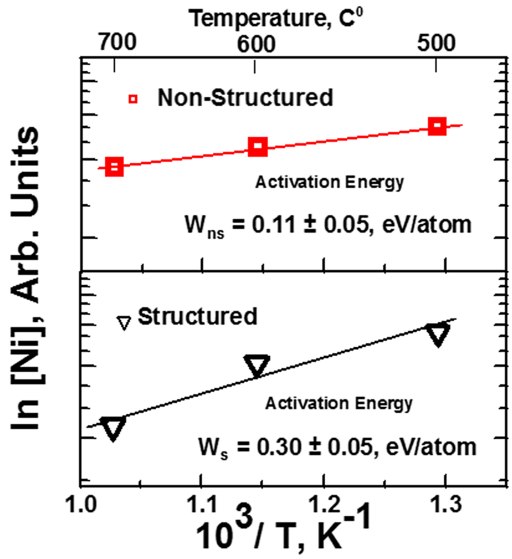

FIG. 5. Nickel concentration as a function of the temperature of the structured and non-structured substrates. The activation energies of the desorption process are indicated.

detaching atoms probability per unit of time (detaching frequency), *i.e.*, $\nu_0=\tau_0^{-1}$, which is of the order of the phonon vibration frequency ($\sim 10^{13}$ Hz).[22] Then, the desorption probability per unit of time is $\nu=\tau^{-1} = \nu_0 \exp(-W/k_BT)$, *i.e.*, ν represents the number of Ni atoms per unit of time evaporating into the deposition chamber. Therefore, larger W values imply less probability for a Ni atom to detach.

From Fig. 5, the activation evaporation energies obtained for the structured and non-structured substrates are W_{ns} = (0.11 ± 0.05) eV/atom and W_s = (0.30 ± 0.05) eV/atom, respectively. Finally, by substituting the evaporation energies W_s and W_{ns} in the detaching probability ratio for the studied substrates defined by $\rho = (\nu_s/\nu_{ns}) = \exp(W_{ns}-W_s)/k_BT$, a value of $\rho \sim (1/20) \sim 5$ % is obtained for T = 500 ^{0}C. This means that Ni atoms stay longer sitting on the structured than in non-structured substrates and thus have more chances to be retained. Finally, we note that the value W_{ns} = (0.11 ± 0.05) eV/atom is comparable to the bulk Ni evaporation energy at $\sim 10^{-4}$ Torr, as reported in the literature.[39,40]

We finish this section including an estimation of $L \sim a_0 \exp(3\phi/2k_BT)$, the mean displacement of absorbed Ni atoms at the temperatures reported in this work. Here a_0 is of the order of the atomic distance and $\phi \sim W/20$, where W is the evaporation energy, and k_BT has the usual meaning.[22] Assuming a_0 =2.34 Å (Si-Si bulk distance) $k_BT \sim 0.075$ eV (T ~600 K), and $W_{ns} \sim 0.11$eV obtained above, the mean displacement is L ~2.6 Å, *i.e.*, of the order of the atomic Si-Si distance.

2. Mean diameter Ni particles size and density distribution: Constant atoms F and variable substrate T. Influence of the substrate

In this sub-section, we shall study the influence the T, at constant F of atoms arriving at the substrate on the diffusion and coalescence of Ni atoms. The diameter and density of the particles obtained on the substrates were obtained from SEM micrographs. The analysis was performed on samples obtained by depositing Ni on both the TiN_xO_y coated structured and non-structured substrates, as discussed in Section II.

Figure 6 shows the influence of the substrate and T on the particles sizes and distribution by the F obtained bombarding the Ni target with 1keV. As discussed above, the size of the Ni particles is determined by a competition between evaporation and the mean displacement L of atoms landing on the substrate before finding a new nucleation site or joining to an existing island. Figure 6(a) shows that for the non-structured substrate the particle average size increases roughly 4X with T_{dep} increasing from 500-700 ^{0}C. Moreover, for the same range of T, the density of particles decreases by a factor ~5/7. These results are consistent with the expression $r \sim F^p/D^q$, *i.e.*, augmenting D diminishes the density of particles. Concomitantly, the average particle size is expected to increase during the annealing process due to coalescence, as observed. We interpret these findings as being governed by thermodynamic effects since higher Ni mobility implied low affinity of the atoms with the substrate, *i.e.*, relative higher desorption probability ν_{ns}.

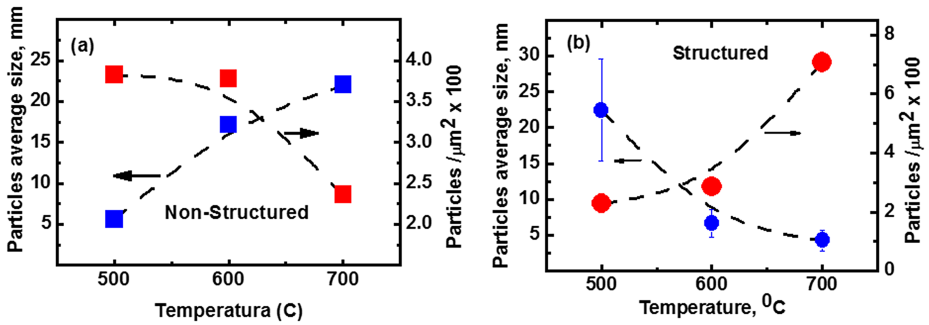

FIG. 6. Average size and density of Ni particles for samples obtained using constant F (obtained for Ar^+ ion bombarding, 1 keV energy) of Ni atoms and variable T onto non-structured (a) and structured (b) Si substrates. Except when indicated, the size of the symbols is of the order of the experimental errors.

Opposite results are found for the size and density of particles deposited on structured substrates due to the strain and defects introduced by the ion bombardment [Figure 6(b)]. First, the sizes of the Ni particles decrease up to four times with T. This is in apparent contradiction with the increased atoms mobility with T, *i.e.*, increasing L the mean distance traveled by the atoms should augment the probability for the atoms to meet an island instead to find a new nucleation site and thus prompting bigger cluster. Second, an unusual behavior is also found for the density of particles evolution: increasing T augments the number of Ni particles up to three times per unit of area. In fact, higher mobility (due to T) should increase the probability of atoms encounters, *i.e.*, the formation of a bigger cluster and thus lower particles density, contrary to what is found. These findings could be understood assuming that a pseudomorphic phenomenon occurred during the films growth and posterior annealing.[41,42] The presence of compressive stress decreases the surface diffusion barriers. On the contrary, tensile stress, increases the diffusion barriers. Intuitively, compressive stress reduces the atomic separation, smoothening the crystalline potential while tensile stress increases the atoms distance resulting in an opposite effect. Moreover, surface stress causes dislocations and defects acting as nucleation centers or repulsive barriers. If is so, the augment of the density of Ni particles with T indicates that the large island breaks in smaller ones due to the instabilities prompted by the strain.[43,44] We shall see later that the asymmetric strain in the structured samples induces the Ni particles organization on the sculpted substrates. In fact, as discussed in Section I, the Ni atoms displacements on the substrate are influenced by elastic driving forces modifying the kinetics of the coalescence. Therefore, the anisotropic stress discussed in Section III will help to understand the Ni organization reported below. As noted above, a compressive stress decreases the atomic separation while a tensile stress moves the atoms apart. In the former case, the interaction of the Ni particles on the surface decreases while in the latter one, an open structure increases the surface interaction, in both cases influencing the displacements L.[41,42] We understand, however, that the phenomenon is complex because the reported strain discussed in this work is an average value on the substrate surface. Therefore, the Ni atoms landing in the valley sites interact, might be, weaker with the substrate being able to hike uphill to reach the top of the hill. Nevertheless, more work is necessary to gain physical insight of the experimental findings reported in this part of the work.

3. Nickel particles distribution at variable F. Influence of the substrate pattern

In this sub-section, we shall study the influence of the substrate on the Ni particles retention on the surface by varying the F of Ni atoms at two different deposition temperatures T followed by the annealing procedure. We remark that to compare island densities requires the same amount of material deposited on the substrate. In fact, this is difficult to obtain because although that F can be maintained constant the final amount of Ni retained depends on the *T* of the substrate. Therefore, the Ni retention is a combined result of the temperature and the state of the state of the surface for each F studied.

Figure 7(a) shows the Ni concentration, as obtained from XPS measurements, as a function of the Ni target bombarding energy for samples deposited at two temperatures (500 and 700 ^{0}C) on a structured substrate. Considering that the sputtering yield increases with the ion bombarding energy, the x-axis could be considered increasing as a function of F.[29] As it is expected, the Ni concentration retained in the surface increases on F (*i.e.*, the supply of Ni atoms) for both studied temperatures (see Section III D, sub–section 1). Moreover, for each bombarding energy, i.e., constant F and equal Ni doses, Figure 7(a) shows that for 700 ^{0}C the Ni concentration retained on the patterned substrate is smaller than the one obtained at 500 ^{0}C, as it is expected. On the other hand, Figure 6(b) shows that the number of particles per unit of area is also larger for samples obtained at ~700 ^{0}C, an expected result considering that more nickel was retained on the sample.

Figure 7(b) shows the Ni surface concentration dependence on the target bombarding energy obtained in samples deposited a constant temperature (700 °C) on structured and non-structured substrates. As observed in the figure the nickel concentration is systematically higher for the samples deposited on structured substrates. Specifically, for each bombarding energy, i.e., constant F, the Ni retained in the substrate is larger on the structured substrate.

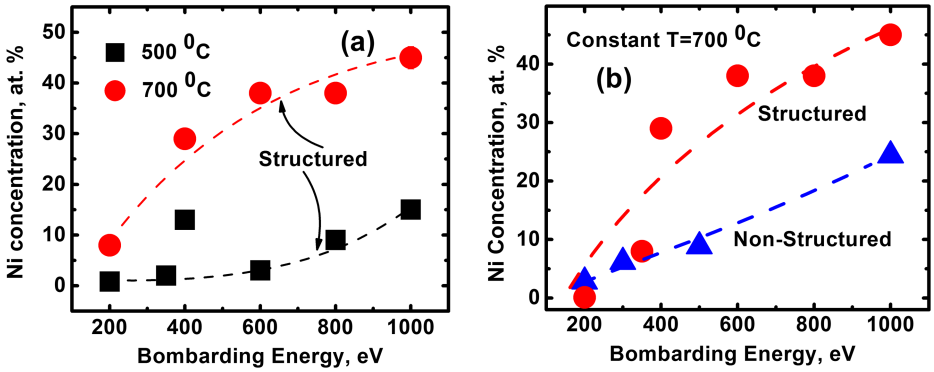

FIG. 7. Nickel concentration (as obtained from XPS measurements) as a function of the sputtering energy of samples deposited at different temperatures and substrates: (a) 700 and 500 °C, structured, and (b) 700 °C, non-structured and structured. In the range of the energies studied, the atoms F increases with the sputtering energy.

As before, this behavior is consistent with the fact that the activation evaporation energy is larger for the nanostructured substrate. Hereby, Ni atoms stay longer wandering on the surface and thus increasing the probably to find a nucleation site before evaporating. This is plausible because as it was shown above, the ratio of the provability of detaching Ni atoms for the structured and non-structured substrate is $\rho = (\nu_s/\nu_{ns}) \sim 5$ %, *i.e.*, it is more favorable for the Ni particles to remain in the structured substrates than in the non-structured ones.

4. Ni particles organization at constant F and variable substrate T. Effect of the substrate

In the previous sections was presented a comprehensive study of both the effect of the ripples on the surface strain of the substrate and its consequences on the Ni particle average size and density as a function of deposition T and F of Ni atoms. Based on this information we are proceeding to discuss the experimental results obtained on the Ni islands organization due to the concomitant effects of the strain and substrate surface's ripples.

Figure 8 shows examples of the Ni particles organization obtained by AFM in a select group of samples. These samples were obtained at constant F and two different T (500 and 700 ^{0}C) on non-structured (a, c) and structured substrates (b, d). The F was constant by fixing the energy (1000 eV) of the Ar^+ ion beam that sputter the Ni target. Different size, surface density, and organization of the particles are evident in both kinds of substrates.

Figures 8(a) and 8(c) show the distribution of Ni particles on the non-structured substrate for two deposition temperatures. The insets (Fast Fourier Transformation - FFT) show that, at the lower T the Ni particles display some sort of order due to the intrinsic strain of the coated and non-structured Si substrate (see Figure 4). This organization can be interpreted as due to the compressive strain diminishing the diffusion barrier in a preferential direction inducing privileged alignment of the Ni atoms.[41,42] Higher deposition temperatures inhibit this process by increasing the probably that Ni atoms overcome the diffusion barriers [Figure 8(c)]. Figure 8(b) shows two characteristic patterns. The first one is a diagonal arrangement of particles. The second one shows a preferential particles deposition along the top of the hills. Indeed, the FFT shows clearly these two quite organized Ni particles arrangement (inset). We associated the patterns with the anisotropic stress shown in Fig. 4: one direction along 0-180^0 and the other one along the 150^0-300^0 orientation. As before, the combined anisotropic stress diminishes the diffusion barrier in the preferential directions observed in the micrograph. Increasing the deposition T, on the other hand, allows the Ni atoms to overcome the diffusion barriers allowing the formation of coarse clusters [Fig. 8(d)]. In this later case, it is interesting to notice that the Ni particles continue to agglomerate along the top of the ripples, suggesting that the experimental conditions were not appropriate as to maintain the Ni particles in the valleys. As it was suggested above, it could be due to a weaker atoms interaction with the substrate in the valleys regions allowing the Ni atoms to crawl uphill where they found a more

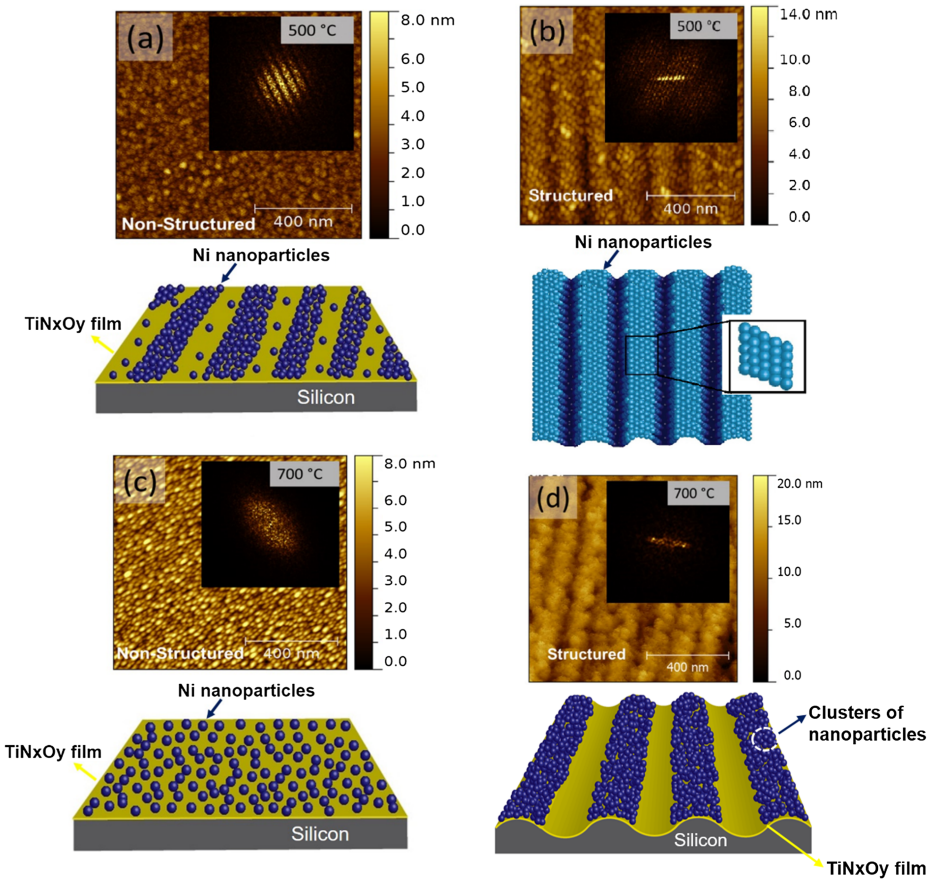

FIG. 8. AFM topographic maps of the nickel particles distribution deposited at constant F on non-structured [(a) and (c)] and structured [(b) and (d)] substrates at 500 and 700°C. The F was maintained constant by fixing the energy (1000 eV) of the Ar^+ ion beam sputtering the Ni target. Insets: Fast Fourier Transforms (FFT) of the corresponding micrographs. Schematic models representing the Ni nanoparticles distribution are displayed below the AFM micrographics (note that the schema do not represent the real size and particles densities). The bottom-up process takes place on the structured pattern surface, prompted by the surface strain (top-down process), and depending on the F/D ratio.

appropriated region to nucleate. Nevertheless, we believe that more work will be necessary to verify this hypothesis.

5. Nickel particles organization at constant substrate T and different metallic atoms F: Effect of the substrate

In this last section, we shall discuss the effect of the F of Ni atoms on the particles organization maintaining the substrate T constant. The preparation parameters of the studied samples are displayed in Table II. The Ni deposition on the TiN_xO_y interfaced on nanostructured substrates were studied at two F. As before, the F was controlled by changing the ion energy bombarding the Ni target (Section II A).

Figure 9 displays the AFM micrographs obtained from some selected samples (200 eV and 1000 eV, Table II) showing the effect of the F on the Ni distribution on the substrate maintaining the substrate T constant (700 ^{0}C). With the purpose of comparison, we have included in this figure the micrographs corresponding to Figs. 8(c) and 8(d) [now identified as Figures 9(c) and 9(d)].

As commented above, no defined pattern of Ni particles deposited on non-structured substrates was obtained under these conditions. For low F (200 eV) the particles are without evident organization and dispersed (i.e., r << 1) [Figure 9(a) and (b)]. For high F (1000 eV) the particles are randomly and densely distributed as expected from the relation $r \sim F^p/D^q$ [Figure 9(c)]. In the case of the structured

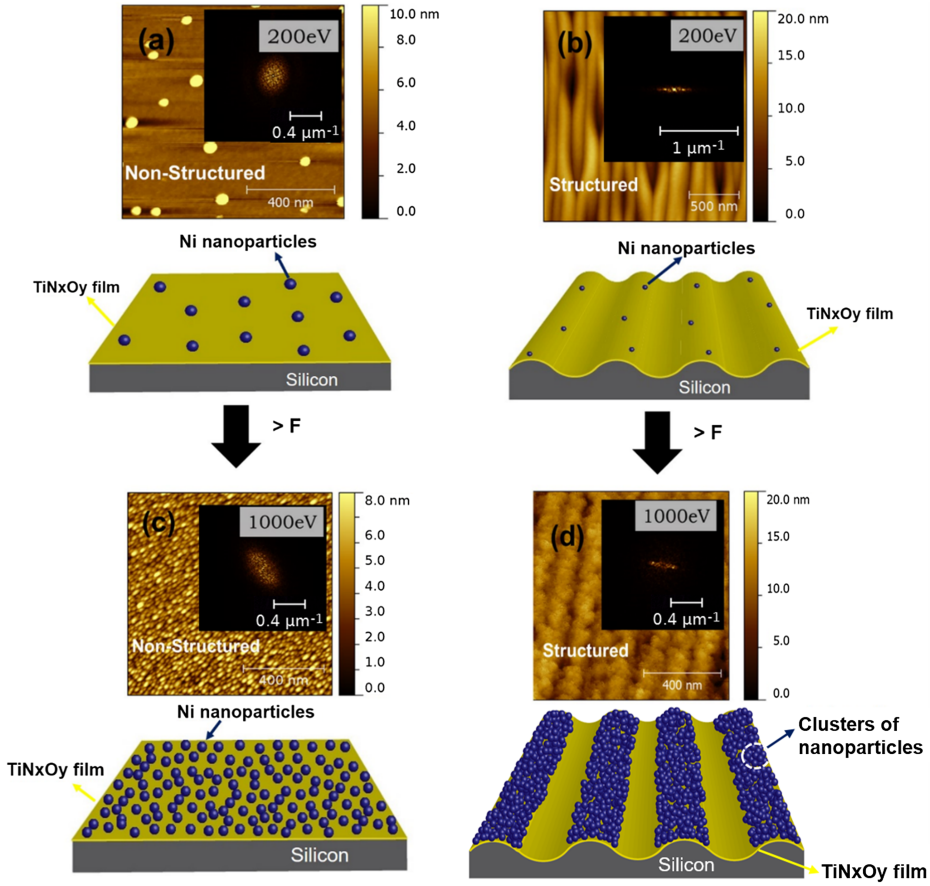

FIG. 9. AFM topographic maps of the nickel particles deposited at constant temperature 700 ^{0}C on substrates intermediated by TiN_xO_y thin film and different metallic atoms F. The F were controlled by the energy of the Ar^+ ion beam sputtering the Ni target. The images correspond to samples obtained by sputtering a nickel target with energies of 200 and 1000 eV onto non-structured [(a) and (c)] and structured [(b) and (d)] substrates. For comparison purposes, Figs 9(c) and 9(d) are the same of Figs 8(c) and 8(d). Insets: Fast Fourier Transform obtained from the micrographs. Models representing the Ni nanoparticles distribution are displayed below the AFM micrographics (note that the schemas do not represent the real size and particles densities). The bottom-up process takes place on the structured pattern surface, prompted by the surface strain (top-down process) and depending on the F/D ratio.

substrates and low F (200 eV) the particles remain highly disperse and its size is so tiny that are not distinguished in the scale of the micrograph. On the other hand, it is remarkable the influence of the Ni atoms F on the nucleation kinetics [Figure 9(c)]. In fact, a relative high Ni atoms F prompts a crowded coarse particles distribution on the top of the ripples, as commented in Section III D, sub–section 4. [Figure 9(d)]

IV. CONCLUSIONS

This work reports a combined in situ sequential top-down and bottom-up ion beam/deposition process prompting self-organization of nanosized metallic particles. The top-down process consists first in Xe^+ ion beam bombardment of crystalline silicon substrates generating regular patterns (nanostructured) followed by depositing a titanium oxynitride thin film to prevent the formation of nickel silicide (diffusion barrier). The titanium oxynitride film presents asymmetric surface strain distribution due to the preferentially transferred momentum along the direction of the ion beam projection on the sample surface and probably defects of the formed pattern. The coalescence of the Ni particles shows two size scales of the organization associated with driving forces stemming from different origins. First, a short scale atomic coalescence due to Ni atoms surface diffusion generating particles

of ~10 Å size. Second, a mesoscale size Ni particles organization that is ascribed to elastic forces prompted by the strain of the TiN_xO_y interface deposited on the sculpted Si, and that can extend hundreds of nanometers. The organized Ni particles are preferentially accommodated on the top and along the ripples. On the top of the hills, approximately 10 particles (~10 Å size) align forming strings interrupted by the valley's ripples making an angle of $\sim 30^0$ relative to the ripples direction. These two main directions organization are associated with the anisotropic surface strain of the sculpted substrate. These conclusions are based on a quantitative study of the effect of T on the Ni atoms diffusion D(T) and the metallic atoms F arriving at the substrate surface. Indeed, the density of the metallic clusters, basically governed by the ratio $r \sim F^p/D^q$, was studied in conditions leading to identify different regimes of coalescence. An important effect prompted by the ripples is the residence lifetime increases of the Ni atoms on the substrate as compared with the non-structured ones. Indeed, for the temperatures studied in the experiments, the lifetime of the Ni atoms on the former substrates was estimated to be around ~20 times longer than the one on the non-structured substrate. These effects are suggested to be due to the larger quantity of nucleation centers prompted by the ions sculpturing employed in the top-down process. Moreover, by increasing the temperature number of Ni particles increases for samples obtained in nanostructured substrates suggesting that the instabilities prompted by the residual strain of the films led the Ni islands to break up forming smaller ones. Also, it is noted that the stressed surfaces probably modify the interaction of the Ni/TiN_xO_y interface and then the coalescence phenomenon. Finally, the results show that it is possible to tailor both the topology and the stress of the crystalline Si substrate by ion bombardment to produce organized patterns of metallic particles.

ACKNOWLEDGMENTS

Part of this work was supported by FAPESP (Project 2012/10127-5). CAF, ARZ and FA are CNPq fellows. SRSM is FAPERGS fellow. X-ray studies were obtained at the National Laboratory of Synchrotron Radiation (LNLS - Brazil). This paper is part of the PhD thesis of MM. The authors are grateful to C. Piacenti for technical assistance.

[1] J. V. Barth, G. Costantini, and K. Kern, Nature **437**, 671 (2005).
[2] B. J. Landi, M. J. Ganter, C. D. Cress, R. A. DiLeo, and R. P. Raffaelle, Energy Environ. Sci. **2**, 638 (2009).
[3] A. Graham, G. Duesberg, R. Seidel, M. Liebau, E. Unger, F. Kreupl, and W. Hönlein, Diamond Relat. Mater. **13**, 1296 (2004).
[4] J. Li, C. Papadopoulos, J. Xu, and M. Moskovits, Appl. Phys. Lett. **75**, 367 (1999).
[5] Y. Yang, S. Huang, H. He, A. W. Mau, and L. Dai, J. Am. Chem. Soc. **121**, 10832 (1999).
[6] R. Bennett, G. Xiong, Z. Ren, and R. Cohen, Chem. Mater. **16**, 5589 (2004).
[7] T. Minea, S. Point, A. Gohier, A. Granier, C. Godon, and F. Alvarez, Surf. Coat. Tech. **200**, 1101 (2005).
[8] J. D. Carey, L. L. Ong, and S. R. P. Silva, Nanotechnology **14**, 1223 (2003).
[9] U. Valbusa, C. Boragno, and F. B. Mongeot, J. Phys. Condens. Mat. **14**, 8153 (2002).
[10] T. Oates, A. Keller, S. Noda, and S. Facsko, Appl. Phys. Lett. **93**, 063106 (2008).
[11] J. Muñoz-García, L. Vázquez, M. Castro, R. Gago, A. R. Cubero, A. M. Barrado, and R. Cuerno, Mat. Sci. and Eng. R **86**, 1 (2014), and references there in.
[12] J. J. Acuña, M. Escobar, S. N. Goyanes, R. J. Canal, A. R. Zanatta, and F. Alvarez, J. Appl. Phys. **109**, 114317 (2011).
[13] S. Cucatti, R. Droppa, Jr., C. Figueroa, M. Klaus, C. Genzel, and F. Alvarez, J. Appl. Phys. **120**, 145306 (2016).
[14] E. Ochoa, C. Figueroa, T. Czerwiec, and F. Alvarez, Appl. Phys. Lett. **88**, 254109 (2006).
[15] F. Cemin, F. G. Echeverrigaray, A. C. Rovani, C. L. Amorim, R. L. Basso, I. J. Baumvol, and C. A. Figueroa, Mater. Sci. Eng. A **527**, 3206 (2010).
[16] C. Davis, Thin Solid Films **226**, 30 (1993).
[17] F. M. d'Heurle and J. M. E. Harper, Thin Solid Films **171**, 81 (1989).
[18] M. Imboden and D. Bishop, Phys. Today **67**, 45 (2014).
[19] M. Imboden, H. Han, T. Stark, E. Lowell, J. Chang, F. Pardo, C. Bolle, P. G. Del Corro, and D. J. Bishop, Nanoscale **6**, 5049 (2014).
[20] Z. Zhang and M. G. Lagally, Science **276**, 377 (1997).
[21] Y. W. Mo, J. Kleiner, M. B. Webb, and M. G. Lagally, Phys. Rev. Lett. **66**, 15 (1998).
[22] W. K. Burton, N. Cabrera, and F. C. Frank, Philos. Trans. R. Soc. Lond. A **243**, 299 (1951); D. Woodruff, *ibid.* **373**, 20140230 (2015).
[23] P. Hammer, N. Victoria, and F. Alvarez, J. Vac. Sci. Technol. A **16**, 2941 (1998).
[24] M. Morales, R. Merlo, R. Droppa, and F. Alvarez, J. Phys. D: Appl. Phys. **47**, 195303 (2014).
[25] A. Biermanns, U. Pietsch, J. Grenzer, A. Hanisch, St. Facsko, G. Carbone, and T. H. Metzge, J. Appl. Phys. **104**, 044312 (2008).
[26] T. K. Chini, F. Okuyama, M. Tanemura, and K. Nordlund, Phys. Rev. B **67**, 205403 (2003).

[27] A. Keller, S. Roβbach, S. Fascko, and W. Möller, Nanotechnology **19**, 135303 (2008).
[28] J. P. Biersack and L. G. Haggmark, Nucl. Instrum. Methods **174**, 257 (1980).
[29] B. N. Chapman, in *Glow discharge processes* (John Wiley & Sons, 1980).
[30] D. Briggs and M. P. Seah, in *Practical Surface Analysis* (John Wiley & Sons, 1996).
[31] C. S. Madi, E. Anzenberg, K. F. Ludwig, Jr., and M. J. Aziz, Phys. Rev. Lett. **106**, 066101 (2011).
[32] S. Facsko, T. Bobek, A. Stahl, H. Kurz, and T. Dekorsy, Phys. Rev. B **69**, 153412 (2004).
[33] M. Castro, R. Cuerno, L. Vázquez, and R. Gago, Phys. Rev. Lett. **94**, 016102 (2005).
[34] R. M. Bradley and J. M. Harper, J. Vac. Sci. Technol. A **6**, 2390 (1988).
[35] W. L. Chang and E. Chanson, J. Appl. Phys. **101**, 213011 (2007).
[36] J. Narayan, P. Tiwari, X. Chen, J. Singh, R. Chowdhury, and T. Zheleva, Appl. Phys. Lett. **61**, 1290 (1992).
[37] V. Gal, P. Gruzin, and G. Yudina, Phys. Status Solidi (A) **15**, 659 (1973).
[38] J. Sehested, J. Catal. **217**, 417 (2003).
[39] J. F. O'Hanlon, in *A user's guide to vacuum technology* (John Wiley & Sons, 2005).
[40] R. E. Honig and D. A. Kramer, RCA Review **30**, 285 (1969).
[41] H. Brune, K. Bromann, H. Röder, K. Kern, J. Jacobsen, P. Stoltze, K. Jacobsen, and J. No, Phys. Rev. B **52**, R14380 (1995).
[42] C. Ratsch, A. P. Seitsonen, and M. Scheffler, Phys. Rev. B **55**, 6750 (1997).
[43] S. Pandya, A. R. Damodaran, R. Xu, S. L. Hsu, J. C. Agar, and L. W. Martin, Sci. Rep. **6**, 26075 (2016).
[44] R. Schuster, H. Röder, K. Bromann, H. Brune, and K. Kern, Phys. Rev. B **54**, 13476 (1996).